Journal of Cleaner Production 373 (2022) 133790

Contents lists available at ScienceDirect

Journal of Cleaner Production

journal homepage: www.elsevier.com/locate/jclepro

Separable amino-functionalized biochar/alginate beads for efficient removal of Cr(VI) from original electroplating wastewater at room temperature

Yingnan He [a,1], Jianbing Chen [b,1], Jiapei Lv [c,1], Yimin Huang [a], Shuxing Zhou [d,***], Wenyan Li [e], Yongtao Li [e], Fengqin Chang [a,**], Hucai Zhang [a], Thomas Wågberg [f], Guangzhi Hu [a,f,*]

[a] Institute for Ecological Research and Pollution Control of Plateau Lakes, School of Ecology and Environmental Science, Yunnan University, Kunming, 650504, PR China
[b] Research Academy of Non-metallic Mining Industry Development, Materials and Environmental Engineering College, Chizhou University, Chizhou, 247000, PR China
[c] State Key Laboratory of Environmental Criteria and Risk Assessment, Chinese Research Academy of Environmental Sciences, Beijing, 100012, PR China
[d] Hubei Key Laboratory of Low Dimensional Optoelectronic Materials and Devices, Hubei University of Arts and Science, Xiangyang, 441053, PR China
[e] Joint Institute for Environmental Research and Education, College of Resources and Environment, South China Agricultural University, Guangzhou, 510642, PR China
[f] Department of Physics, Umeå University, S-901 87, Umeå, Sweden

ARTICLE INFO

Handling Editor: Prof. Jiri Jaromir Klemeš

Keywords:
Sodium alginate gel beads
Polyethyleneimine modification
Biochar
High capacity
Hexavalent chromium removal
Room temperature adsorption

ABSTRACT

An alginate gel bead composite adsorbent with polyethyleneimine (PEI) as a surface modifier and *Eichhornia crassipes* (EC) biochar, known as EC-alg/PEI-3, was added internally to the adsorb Cr(VI) from an aqueous environment. The functionalized gel beads were characterized using SEM, XPS, FTIR, and other techniques. The maximum adsorption capacities of EC-alg/PEI-3 were 714.3 mg g^{-1} at 10 °C and 769.2 mg g^{-1} at 25 °C. In the treatment of highly concentrated electroplating wastewater, EC-alg/PEI-3 can be dosed at 1.4 g L^{-1} to reduce the concentration of Cr(VI) to below 0.05 ppm. EC-alg/PEI-3 maintained a competitive adsorption capacity after six cycles. This spherical adsorbent material is easy to prepare, has a very high adsorption capacity, is environmentally friendly, and can be easily recycled. The EC-alg/PEI-3 gel beads are promising for the treatment of industrial wastewater.

1. Introduction

Chromium (Cr) is considered one of the most toxic heavy metals found in nature and is widely used in many industrial processes, such as metallurgy, welding, metal finishing, and tanning (Qu et al., 2021; Sharma et al., 2022). Cr exists mainly in the form of Cr(III) and Cr(VI). Cr (VI) is 100 times more toxic than Cr(III) in aqueous environments. Cr(VI) is mainly present in water column as $Cr_2O_7^{2-}$, CrO_4^{2-}, $HCrO_4^-$, and other soluble anions (Kong et al., 2022; Sivaraman et al., 2022), which have strong oxidation and migration capacities. When the concentration of Cr (VI) in drinking water is higher than 0.10 ppm, it causes symptoms such as heavy metal poisoning, carcinogenesis, and mutagenesis. There are several ways to reduce the concentration of Cr(VI) in water bodies, including adsorption (Bajpai et al., 2004), electrochemistry (Chen et al., 2021), membrane treatment (Han et al., 2022), and bioremediation (González et al., 2012). Adsorption has the advantages of simple operation and wide application and is considered to be a competitive treatment technology for dealing with heavy metal pollution in aqueous environments. Common adsorbents such as biochar, graphene, carbon nanotubes, and metal-organic frameworks are mostly in the form of nanoscale powders, which are usually modified using metallic materials or organic substances. In practical scenarios, there are problems with metal leaching and difficulties in the secondary recovery of nanomaterials. Therefore, there is a need to identify suitable embedding materials to immobilize nanomaterials in suitable matrices.

Natural polysaccharide polymeric materials are gaining increasing

* Corresponding author. Institute for Ecological Research and Pollution Control of Plateau Lakes, School of Ecology and Environmental Science, Yunnan University, Kunming, 650504, PR China.
** Corresponding author.
*** Corresponding author.
E-mail addresses: sxzhou@hbuas.edu.cn (S. Zhou), changfq@ynu.edu.cn (F. Chang), guangzhi.hu@umu.se (G. Hu).
[1] These authors contributed equally.

https://doi.org/10.1016/j.jclepro.2022.133790
Received 8 April 2022; Received in revised form 19 August 2022; Accepted 21 August 2022
Available online 26 August 2022

attention from researchers because they are easily available without toxic effects, have adjustable surface morphologies and physicochemical properties, have a high affinity for heavy metals, and undoubtedly have great potential to become green and efficient adsorbents (Guan et al., 2022). Among them, alginate is a low-cost, easily manufactured material rich in carboxyl groups. Sodium alginate (SA) is a common natural linear anionic polysaccharide containing mainly β-1,4-glycosidic linkages of α-l-mannuronic acid and β-d-gulo-guluronic acid, which are highly biocompatible and biodegradable and form gels of a certain size and shape (filamentous, beads, membrane) by cross-linking with divalent or trivalent metal ions (Fan et al., 2020). However, the weak mechanical strength and low adsorption capacity of SA affect its applicability in the adsorption process. Therefore, the introduction of inorganic/organic fillers into the SA matrix both improves the mechanical weaknesses of the original SA (Asnam et al., 2022), and the fillers can have a synergistic effect with the SA matrix in terms of durability and adsorption properties. SA has been widely used to immobilize small particle materials such as biochar (Qiao et al., 2020), clay materials (Lin et al., 2021), graphene oxide (Zhuang et al., 2016), and metal-organic frameworks (Jia et al., 2022). Lv et al. (2017) synthesized reduced graphene oxide-alginate beads with embedded FeO nanoparticles. Compared to unmodified SA beads, the breakage rate decreased by 40% under shaking at 500 rpm for 30 days, and the removal rate of Cr(VI) was improved by 65% within 3 h. Zhang et al. (2019) prepared alginate-encapsulated multi-chambered triethylenetetramine -modified chitosan beads for the removal of Cr(VI). Under optimal experimental conditions, the maximum Cr(VI) adsorption was 291.3 mg g^{-1}, which was approximately 11 times higher than that of pure alginate beads.

In the present work, functionalized SA gel beads prepared by a simple method are proposed for Cr(VI) removal from the aqueous humor. Porous biochar was prepared using $MgCl_2$-modified *Eichhornia crassipes* (EC). The porous biochar was then thoroughly mixed with the SA gel and dropped into a $CaCl_2$ solution to form gel beads. Subsequently, polyethyleneimine (PEI) was grafted onto the bead surface using glutaraldehyde as a cross-linking agent to increase the amino content of the bead surface and enhance the adsorption of Cr(VI) The adsorbent has a 'core-shell' bead structure, which avoids the supermicron size problems of the adsorbent material and the difficulties of separation and recovery. The prepared gel beads were characterized in various ways, and a series of adsorption experiments were carried out.

The effects of pH, adsorption kinetics, adsorption isotherms, adsorption thermodynamics, and recoverability of the gel beads were discussed. The mechanism of Cr(VI) adsorption during this process was investigated using X-ray photoelectron spectroscopy (XPS) and Fourier transform infrared spectroscopy (FTIR). Furthermore, as it is important to examine the practical application performance of gel beads because of their use in the adsorption of Cr(VI) in water bodies, the adsorption of gel beads in untreated electroplating wastewater solutions was investigated. This study provides information on green and efficient adsorbent that can be applied to practical wastewater treatment.

2. Materials and methods

The materials and characterization methods used for the experiments conducted are described in the Supplementary information (SI).

2.1. Preparation of EC-alg/PEI gel beads

EC powder (4 g) was added to 1 M 40 mL $MgCl_2{\cdot}6H_2O$ solution and mixed at 75 °C for 12 h. Subsequently, the mixture was dried, ground, and thermally decomposed at 10 °C min^{-1} under N_2 atmosphere and maintained at 500 °C for 2 h to obtain Mg-modified biochar. The resultant biochar was stirred with 1 M HCl for 24 h to remove the Mg ions and ash, and the acid-washed biochar was washed to a neutral pH with plenty of water. After dissolving SA (0.5 g) in 25 mL of deionized (DI) water, an equal amount of the modified EC biochar was added and mixed for 24 h. The mixed solution was added dropwise to a 2% (w/v) $CaCl_2$ solution to obtain EC-alg gel beads, which were left for 24 h.

The gel beads were cleaned and soaked with DI water to wash away excess Ca^{2+} and Cl^- and immediately transferred to 100 mL of different masses of PEI solution while stirring for 6 h. They were then rapidly transferred to 100 mL of 2% glutaraldehyde aqueous solution to cross-link with PEI and stirred at 50 °C for 1 h. The gel beads were filtered and cleaned alternately by ethanol and DI water to remove unreacted glutaraldehyde. The gel beads were frozen for 30 min and then vacuum freeze-dried for 12 h. To select the optimal PEI modification amount, 0.5, 1.5, 3, 4, and 5 g of PEI were added, and the obtained gel beads were named EC-alg/PEI-0.5/1.5/3/4/5, respectively.

2.2. Batch adsorption

The adsorption behavior of EC-alg/PEI was investigated through batch adsorption experiments, including the solution pH, adsorption time, and temperature. A typical adsorption test involved the addition of 0.012 g of adsorbent to 30 mL of Cr(VI) solution and dynamic adsorption at 150 rpm. All tests were repeated three times.

First, the influence of the initial pH on Cr(VI) adsorption was investigated. Cr(VI) solution with a concentration of 200 ppm was prepared by changing the pH to 1.5–8.0 with 0.1 M HCl and 0.1 M NaOH. To investigate the time required to reach adsorption equilibrium, 300 mL of Cr(VI) solution with initial concentrations of 200 and 1000 ppm and pH 2.0 were used and 0.5 mL of the solution was collected at different times. The adsorption isotherms were measured at 10, 25, and 40 °C, and the initial concentration of Cr(VI) was varied between 200 and 1,400 ppm. Cr solutions were measured by Inductively Coupled Plasma Optical Emission Spectrometer (ICP-OES) and UV spectrophotometer was used to measure the concentration of Cr(VI). The remaining Cr(VI) concentration was calculated from the absorbance at 540 nm and the calibration curve of the UV–Vis spectrophotometer, using diphenylcarbazide (DPC) as a color developer. The equilibrium adsorption capacity q_e (mg g^{-1}) was calculated as

$$q_e = \frac{(C_0 - C_e)\cdot V}{m} \quad (1)$$

where C_0 (ppm) and C_e (ppm) were the initial and equilibrium concentrations; V (L) was the volume of the initial solution; and m (g) was the mass of the adsorbent.

2.2.1. Adsorption of Cr(VI) in electroplating wastewater

Using untreated electroplating wastewater from the Jiangyan Longgou Electroplating Factory (Taizhou City, 161 Jiangsu Province, China), a test experiment for the practical application of EC-alg/PEI-3 was conducted. First, 12 mg EC-alg/PEI-3 was added to 30 mL of untreated electroplating wastewater and the experiment was performed at 25 °C until reaching adsorption equilibrium. The Cr(VI) concentration in the wastewater before and after adsorption was tested. Finally, 12 mg of EC-alg/PEI-3 was added to 30 mL of untreated plating wastewater and tested at 25 °C until adsorption equilibrium was reached.

2.2.2. Desorption experiments

Adsorption was carried out at 25 °C for 24 h at pH 2.0, with 200 ppm Cr(VI). The gel beads were filtered and shaken with 50 mL of 0.1 M HCl solution for 30 min to wash away the Cr(III) and then with 50 mL of 0.1 M NaOH solution for 30 min. The surface of the gel beads was then rinsed with DI water until neutral pH was achieved. Another 30 mL of the Cr(VI) solution was added for the subsequent adsorption experiment. This procedure was repeated six times.

3. Results and discussion

The behavior, mechanism and application of EC-alg/PEI-3 on the

adsorption of Cr(VI) in solution were analyzed by the relevant characterization and experimental results.

3.1. SEM analyses

Digital photographs and SEM images of the EC-alg/PEI-3 beads are shown in Fig. 1. The EC-alg/PEI-3 beads were uniform in size, with an average diameter of approximately 2 mm (Fig. 1a). The EC biochar was embedded in the alginate gel layer and exhibited an irregular surface and porous structure with different pore sizes (Fig. 1e). The 3D porous structure inside the gel beads can be observed in the bead cross-section, which has an 'egg-box' structure formed by calcium alginate (Karthik and Meenakshi, 2015). The EC-alg/PEI-3 beads exhibited a spherical "core-shell" structure with a rough surface (Fig. 1d and g) which proves that PEI was successfully grafted onto the surface of the EC-alg gel beads. The porous structure of the EC-alg/PEI-3 beads facilitates the diffusion of Cr(VI) and provides active sites for Cr(VI) adsorption. After the adsorption of Cr(VI), the EC-alg/PEI-3 beads maintained their robust 3D porous structure, but the surface became rough, probably because the adsorbed Cr(VI) partially filled the porous channels.

3.2. BET analyses

To explore the relationship between the pore size and specific surface area of the gel beads and adsorption, N_2 adsorption–desorption experiments were performed. The resulting adsorption isotherms represented typical type-IV adsorption isotherms according to the IUPAC classification (Zhao et al., 2021). The SA and EC-alg/PEI-3 beads were shown to have mesoporous and microporous structures with H_2 hysteresis lines, which also indicated the formation of calcium alginate gels with a reticulate structure. In contrast to the SA beads (Fig. 2b), the surface area of EC-alg/PEI-3 increased slightly from 50.07 $m^2\ g^{-1}$ to 51.8 $m^2\ g^{-1}$, the pore size increased significantly from 12.1 nm to 26.4 nm and the pore volume increased approximately 2.3 times (0.15–0.34 $cm^3\ g^{-1}$). This may be attributed to the doping of the gel beads with Mg-assisted open pore EC biochar. After modification with the Mg, the EC biochar underwent a decomposition process of $MgCl_2$ during pyrolysis, releasing HCl and H_2O and causing the formation of pore structures in the biochar matrix (Yin et al., 2021). During the pyrolysis process, newly formed MgO and (MgOH)Cl can be used as in situ templates for generating porous structures in the biochar matrix, and after acid washing, the template sites are exposed to form a larger surface area (Ling et al., 2017). The specific surface area of the Mg-modified EC biochar powder was 308.120 $m^2\ g^{-1}$, which is much larger than that of the unmodified biochar (79.711 $m^2\ g^{-1}$). The EC-alg/PEI-3 composite had more active sites and facilitated the access of contaminants to the surface and interior of the adsorbent. After the adsorption of Cr ions, the specific surface area, pore size, and pore volume decreased slightly to 50.72 $m^2\ g^{-1}$, 23.9 nm, and 0.30 $cm^3\ g^{-1}$, respectively, which may be caused by the adsorbed Cr(VI) occupying some of the pore channels.

3.3. XPS analyses

The XPS spectra of EC-alg/PEI-3 before and after adsorption are shown in Fig. 3. The peaks at 399.3 eV and 398.5 eV shown in Fig. 3d were attributed to $–NH_2$ and = N groups (Yan et al., 2017). A new peak, corresponding to the protonated amine group appeared at 400.9 eV after adsorption. The protonation of the active amine site on the surface of EC-alg/PEI-3 at a lower pH might have increased the number of positive charges on the surface of the material, making it more favorable for binding Cr(VI). Following Cr(VI) adsorption (Fig. 3e), the binding energies of the $–NH_2$ and = N groups moved correspondingly to 399.6 eV and 398.3 eV, indicating the involvement of these functional groups in the adsorption process. Furthermore, from the inverse fold product of

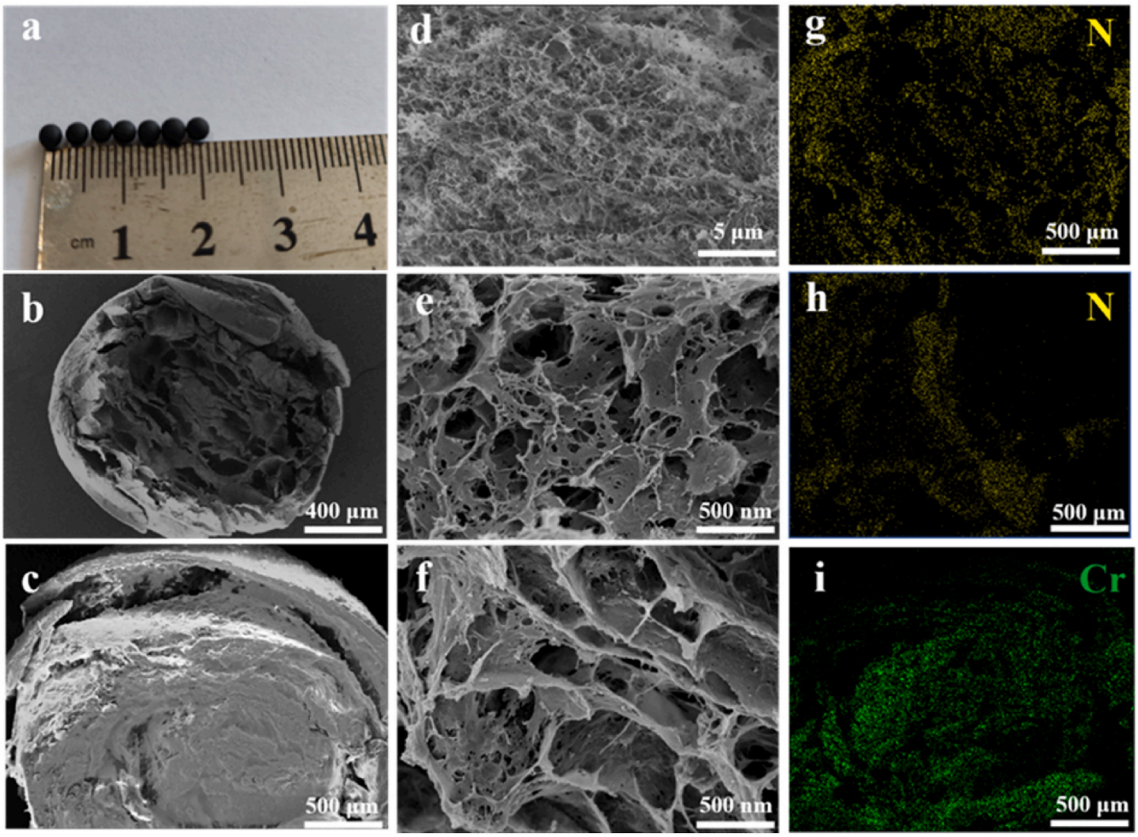

Fig. 1. Digital photo of EC-alg/PEI-3 **(a)** and SEM images of the EC-alg/PEI-3 bead cross-section **(b, e)** and surface SEM image before **(d)** and after Cr(VI) adsorption **(c, f)**; EDS elemental mapping of the EC-alg/PEI-3 beads **(g, h)** and after Cr(VI) adsorption **(i)**.

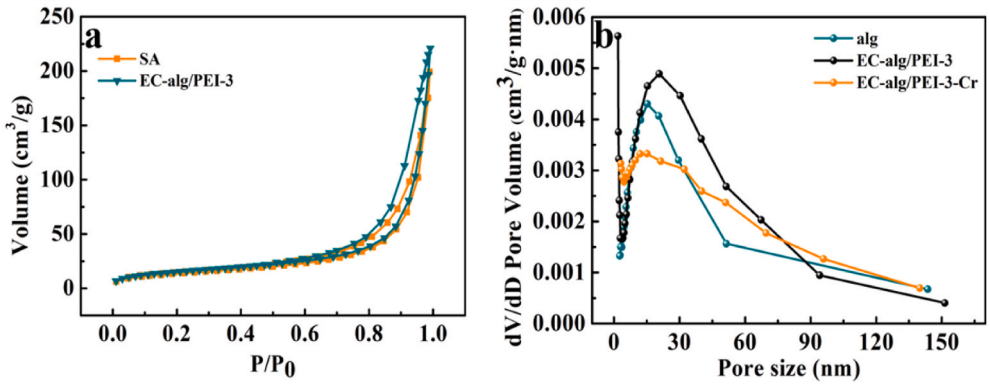

Fig. 2. N_2 adsorption–desorption isotherm curves and pore distribution of SA beads and EC-alg/PEI-3 beads **(a)**, pore size of alg and EC-alg/PEI-3 before and after Cr (VI) adsorption **(b)**.

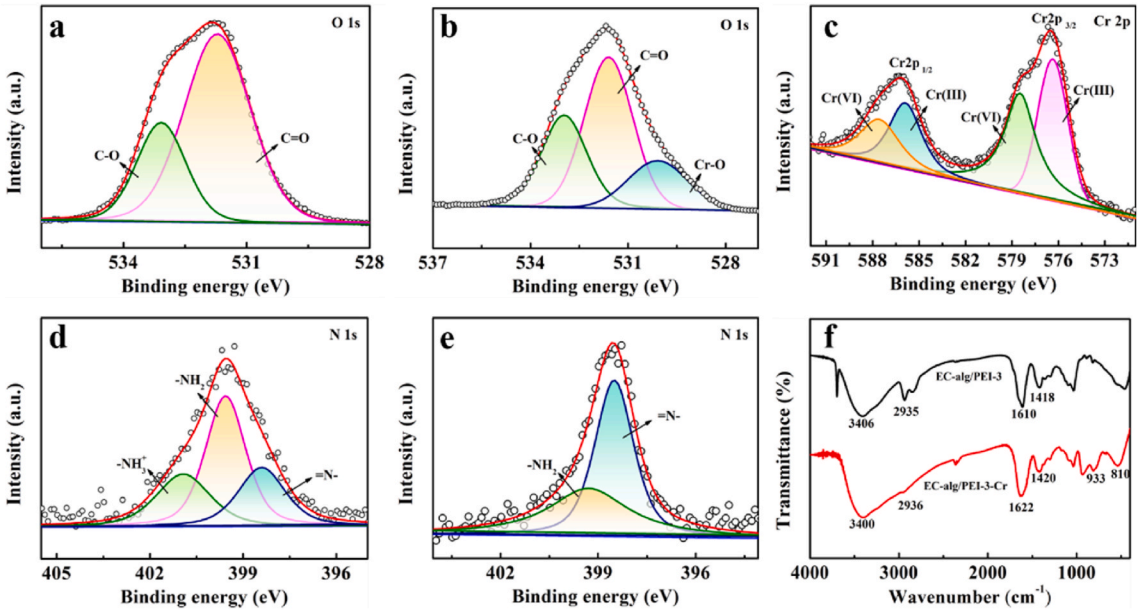

Fig. 3. Spectra of O 1s of EC-alg/PEI-3**(a)** and EC-alg/PEI-3-Cr **(b)**; the high-resolution Cr $_{2p}$ spectrum of EC-alg/PEI-3-Cr **(c)**; the N 1s spectra of EC-alg/PEI-3 **(d)** and EC-alg/PEI-3-Cr **(e)**; FTIR spectra of EC-alg/PEI-3 and EC-alg/PEI-3-Cr specimens **(f)**.

the O 1s spectra of Fig. 3a and b, the two peaks associated with C–O and C=O at 531.7 eV and 533.1 eV (Zhang et al., 2019) were shifted to lower binding energies of 513.6 eV and 532.9 eV, respectively, while a new peak at 530.2 eV appeared after adsorption, possibly representing Cr–O. This suggests that Cr may be bound to oxygen-containing groups.

After adsorption (Fig. 3c), EC-alg/PEI-3-Cr showed $Cr2p_{1/2}$ and $Cr2p_{3/2}$ peaks at 586 eV and 576 eV, respectively, showing that Cr(VI) was adsorbed onto the gel beads (Omer et al., 2019). The peaks for $Cr2p_{1/2}$ and $Cr2p_{3/2}$ can be further split into 587.7 eV and 585.9 eV, 578.5 eV and 576.4 eV for Cr(VI) and Cr(III), respectively.

3.4. FTIR analysis

In Fig. 3f, the broad absorption peak at 3406 cm^{-1} originates from the stretching of –OH in SA and EC biochar and the overlapping stretching of N–H groups in PEI. The antisymmetric and symmetric vibrations of COO^- at 2935 cm^{-1} occurred at 1610 and 1418 cm^{-1}, respectively, overlapping the primary and secondary ammonia in PEI (Xiong et al., 2018; Zhao et al., 2017). The signal positions and intensities of the nitrogen- and oxygen-containing groups adsorbed after Cr(VI) were slightly shifted and changed, respectively, suggesting that these groups may be engaged in the adsorption of Cr(VI). For example, a wider and stronger band appears near 3400 cm^{-1}, which may be attributed to the formation of a new hydrogen bond between the –OH group and Cr(VI). The peak at 2936 cm^{-1} was due to alkyl C–H stretching, which decreased in intensity after adsorption, indicating the involvement of C–H in the removal of Cr(VI). New characteristic peaks appeared at 933 and 810 cm^{-1}, which were likely caused by the formation of Cr–O compounds owing to the formation of Cr(III)–NH_2 coordination bonds (Sun et al., 2010, 2014).The N–H bands located at 1610 and 1418 cm^{-1} were later shifted to 1622 and 1420 cm^{-1}.

3.5. Effect of pH on Cr(VI) removal

The effect of the initial pH of the solution on the adsorption can be explained by the form of chromium ions present in the solution and the charge carried on the surface of the adsorbent. In aqueous solutions, Cr ions are usually present in different forms under different pH conditions. When the pH is less than 2, Cr(VI) is mainly present as H_2CrO_4, which is difficult to be adsorbed by electrostatic attraction; when the pH is between 2 and 3, $HCrO_4^-$ is the main form of Cr(VI), and when the pH exceeds 6.8, $HCrO_4^-$ is converted to CrO_4^{2-}. In Fig. 4a, the adsorption

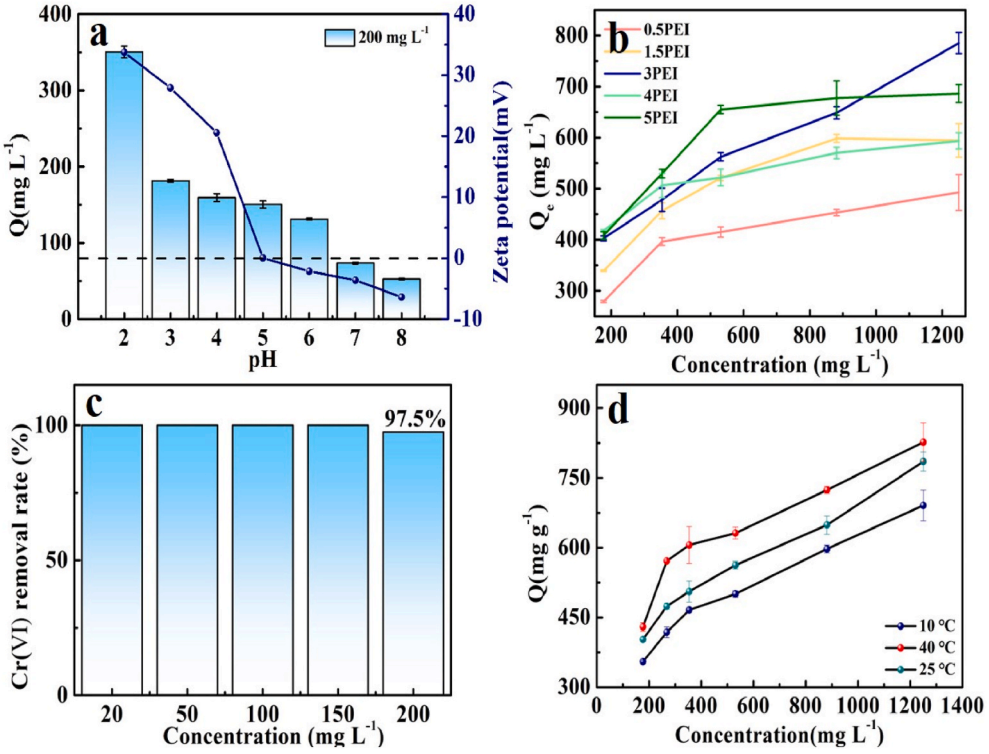

Fig. 4. Adsorption of Cr(VI) by EC-alg/PEI-3 at different pH **(a)**; Adsorption isotherm of Cr(VI) onto the EC-alg/PEI-0.5, EC-alg/PEI-1.5, EC-alg/PEI-3, EC-alg/PEI-4, and EC-alg/PEI-5 **(b)**; Changes in the removal rate of Cr(VI) by EC-alg/PEI-3 with the initial concentration of Cr(VI) **(c)**; Adsorption capacity variation in EC-alg/PEI-3 with the initial Cr(VI) concentration **(d)**.

decreased with increasing pH, reaching a maximum of 350.5 mg g^{-1} at pH 2. This can be attributed to the following. (1) the ionic size of CrO_4^{2-} is larger than that of $HCrO_4^-$ and therefore at pH 2–3 $HCrO_4^-$ ions diffuse more easily in the solution, which facilitates the adsorption. At the same time, when the pH increases, the OH^- concentration in the solution increases, which in turn hinders the diffusion of $HCrO_4^-$ and CrO_4^{2-}, and the OH^- and Cr(VI) anions compete together for the active site of electrostatic attraction, causing the adsorption amount to decrease continuously. (2) The pH_{PZC} of EC-alg/PEI-3 was positive at pH 2–5 (Zheng et al., 2022) and showed a maximum at pH 2 and a negative value at pH 6–8. This suggests that EC-alg/PEI-3 contains a large number of amino and carboxyl groups, which protonate under acidic conditions, making the material positively charged and facilitating Cr(VI) removal from aqueous solutions. (3) A large amount of H^+ is present in the solution at low pH, which is available for the reduction of Cr(VI) to Cr(III) (Pi et al., 2021). When the pH increases, the concentration of H^+ involved in the reduction reaction decreases, resulting in a subsequent decrease in the reduction and removal of Cr(VI) (**Equations 12 and 13**).

3.6. Adsorption isotherms

Adsorption experiments were conducted at room temperature (25 °C, 150 rpm),with shaking at pH 2.0. The adsorption isotherms of EC-alg/PEI-0.5/1.5/3/4/5 were obtained by varying the initial Cr(VI) concentration from 200 ppm to 1400 ppm, and the results are shown in Fig. 4b. The grafting rate of PEI as a functional reagent on EC-alg beads was a key factor in determining the saturation adsorption capacity of the adsorbent for Cr(VI). By using more PEI during synthesis, more amino groups adhered to the EC-alg bead surface through cross-linking. Therefore, the total adsorption of Cr(VI) tended to increase when the amount of PEI was increased to 3.0 g from 0.5 g. Total Cr(VI) adsorption exhibited an increasing trend, however, when the amount of PEI was added from 3.0 g to 5.0 g, the adsorption of Cr(VI) decreased slightly. This was probably because the EC-alg/PEI surface was too dense to expose the adsorption sites (amino or imino), making it difficult to bind to the metal ions (Yan et al., 2017).

The adsorption of Cr(VI) by the beads increased with the initial concentration of Cr(VI), and the adsorption of EC-alg/PEI-3 was higher than that of the other PEI loadings at 769.2 mg g^{-1}. Therefore, EC-alg/PEI-3 was selected for subsequent experiments. The parameter data calculated using the Langmuir and Freundlich models are presented in Table 1.

Freundlich model equation:

$$\log q_e = \log K_F + \frac{1}{n}\log C_e \tag{4}$$

where q_m is the maximum adsorption capacity (mg g^{-1}), q_e is the equilibrium adsorption capacity (mg g^{-1}), C_e is the concentration of Cr

Table 1
Parameters of the Langmuir and Freundlich isotherms for EC-alg/PEI beads with different PEI contents.

$$\frac{C_e}{q_e} = \frac{1}{q_m}C_e + \frac{1}{K_L q_m} \tag{2}$$

$$R_L = \frac{1}{1 + KC_0} \tag{3}$$

		Langmuir			Freundlich		
PEI	q_{max}	K_L	R_L	R^2	K_F	$1/n$	R^2
g	mg g^{-1}	L mg^{-1}			mg g^1		
0	70.4	0.015	0.200–0.800	0.891	7.7	0.354	0.922
0.5	526.3	0.015	0.051–0.274	0.997	137.6	0.186	0.949
1.5	645.2	0.032	0.024–0.260	0.996	74.8	0.343	0.989
3	769.2	0.015	0.051–0.274	0.980	308.2	0.115	0.806
4	588.2	0.041	0.019–0.121	0.994	366.9	0.064	0.941
5	699.3	0.047	0.017–0.107	0.998	331.8	0.109	0.946

Langmuir model equation.

(VI) in the adsorption equilibrium solution (ppm), K_L is the adsorption equilibrium constant (L mg^{-1}), and K_F is the adsorption capacity (g L^{-1}). R_L is the Langmuir dimensionless constant separation factor.

The amount of Cr(VI) adsorbed by EC-alg/PEI-3 increased with temperature (Fig. 4d). The maximum adsorption amounts obtained for EC-alg/PEI-3 using the Langmuir model were 714.3, 769.2, and 833.3 mg g^{-1} at 10, 25, and 40 °C, respectively. The remaining Cr(VI) concentration in solution after adsorption using EC-alg/PEI-3 was negligible at initial concentrations below 200 ppm (Fig. 4c), indicating several easily accessible adsorption sites for this highly efficient adsorption performance composite. The R_L values obtained from the Langmuir model were in the range of 0–0.8, indicating that the sorption process occurred easily. The empirical constants 1/n calculated in the Freundlich model were in the range of 0.1–0.5, which is consistent with the conclusions drawn from the Langmuir model. From the R^2 values in Table 2, both models are suitable for fitting the experimental data, indicating that the adsorption of Cr(VI) by EC-alg/PEI-3 is a complex process rather than simple single-layer adsorption or multiple adsorptions.

The maximum adsorption capacity of gel beads at low and ambient temperatures is of interest when considering practical application scenarios for wastewater treatment. The maximum adsorption capacity of EC-alg/PEI-3 at 25 °C of 769.2 mg g^{-1} was higher than many similar adsorbents in Table 3, whereas the maximum adsorption capacity at 10 °C was only 55 mg g^{-1} lower than that at 25 °C. This also indicates that EC-alg/PEI-3 has a wide useable temperature range and thus excellent prospects for practical applications.

3.7. Adsorption kinetic

The kinetics of Cr(VI) adsorption by EC-alg/PEI-3 was investigated based on the effect of contact time.

As shown in Fig. 5a, at an initial Cr(VI) concentration of 200 ppm, the adsorption capacity reached 50% of the saturation adsorption capacity after 360 h, and the final adsorption equilibrium was reached at 4380 h. At a Cr(VI) concentration of 1000 ppm, 82% of the maximum adsorption capacity was achieved within 24 h. It is probable that the higher concentration of Cr(VI) reduced the mass transport resistance of Cr ions at the interface and increased the effective contact area of the gel beads. This was same as the results shown in Fig. S1, where the R_L value decreased with increasing initial Cr(VI) concentration, showing that Cr (VI) was more readily adsorbed at higher concentrations (Sun et al., 2021).

To understand the adsorption kinetics, the pseudo-first-order (PFO), pseudo-second-order (PSO), intra-particle diffusion and Boyd models were used. The parameter values calculated using the kinetic model are listed in Table 4. The R^2 values obtained using the PSO kinetic model (0.996 and 0.999) were higher than those obtained using the PFO kinetic model (0.944 and 0.913). Furthermore, the PSO model using the q_e values obtained was closer to the model generated in the experiment. This suggests that Cr(VI) sorption by EC-alg/PEI-3 is mainly controlled by chemical interactions rather than material transport (Zhao et al., 2021) (see Table 5).

Pseudo-first order (PFO):

$$ln(q_e - q_t) = \ln(q_e) - K_1 t \tag{5}$$

Table 2
Data for adsorption of Cr (VI) on EC-alg/PEI-3 at different temperatures.

		Langmuir			Freundlich		
T	q_{max}	K_L	R_L	R^2	K_F	1/n	R^2
(°C)	mg g^{-1}	L mg^{-1}			L mg^{-1}		
10	714.3	0.013	0.058–0.310	0.985	189.8	0.179	0.966
25	769.2	0.015	0.051–0.274	0.980	308.2	0.115	0.806
40	833.3	0.030	0.026–0.160	0.989	453.5	0.102	0.918

Pseudo-second order (PSO):

$$\frac{t}{q_t} = \frac{1}{K_2 q_e^2} + \frac{1}{q_e} t \tag{6}$$

Intra-particle diffusion (IPD):

$$q_t = K_i t^{1/2} + C \tag{7}$$

Boyd model:

$$ln\left(1 - \frac{q_t}{q_e}\right) = \ln\left(\frac{6}{\pi^2}\right) - \left(\frac{D}{r^2}\right)\pi^2 t \tag{8}$$

where q_e is the adsorption capacity at equilibrium (mg g^{-1}), q_t is the adsorption capacity at the contact time t (mg g^{-1}), t is the contact time (min), and K_1 (min^{-1}) and K_2 (g mg^{-1} min^{-1}) are the rate constant of pseudo first-order and second-order adsorption. D (cm^2 s^{-1}) is the effective liquid film diffusion coefficient of the sorbents and r (cm) is the radius of the EC-alg/PEI-3 beads (0.1 cm).

During adsorption, heavy metal ions first move from the solution to the outer surface of the adsorbent (membrane diffusion), then from the surface to the interior of the adsorbent (intra-particle diffusion) and are finally adsorbed in the internal structure of the porous adsorbent. According to Fig. 5b (see Table S1 for specific values), the adsorption curve is divided into three straight-line segments that do not pass through the origin, indicating the inclusion of the outer surface, transition phase and the final equilibrium phase. The diffusion rate constants are $K_1 > K_2 > K_3$ and did not pass through the origin, indicating that intra-particle diffusion was not the only rate-limiting step. Due to the instantaneous accessibility of the active binding sites on the EC-alg/PEI-3 surface, higher K_1 values indicated faster adsorption rates in the initial phase. K_1 is significantly higher than K_2 and Cr(VI) takes 120 min to diffuse through the outer surface and 480 min to diffuse through the film before entering the intra-particle diffusion step. In many cases, the adsorption kinetics can be controlled by both film diffusion and intra-particle diffusion (Kapur and Mondal, 2013). According to the Boyd model fit (Fig. 5e), the fitted line does not pass through the origin and the film diffusion coefficient is 10^{-7} for both high and low concentrations, indicating that film diffusion is the main rate-limiting step (Öztürk., 2014), followed by intra-particle diffusion, but other mechanisms such as surface chemisorption may also occur simultaneously (Huang et al., 2018).

3.8. Adsorption thermodynamics

When the temperature rises within the studied temperature range, the amount of adsorption increases; therefore, a higher temperature is beneficial for adsorption. Therefore, the data at three temperatures (10, 25, and 40 °C) were used to establish the thermodynamic parameters of the Cr(VI) adsorption process.

$$\Delta G^o = -RT \ln K_c = \Delta H^0 - T\Delta S^0 \tag{9}$$

$$\ln K_c = \frac{\Delta S^o}{R} - \frac{\Delta H^o}{RT} \tag{10}$$

where *Kc* is a parameter obtained by the Langmuir model, but since the units of K_L in the Langmuir formula used are L mg^{-1}, it needs to be converted to L mol^{-1}, $K_C = K_L \times 1000 \times M_{Cr}$, and T is the temperature (K). Linear regression with T and ΔG^0 was plotted to obtain ΔS^0 and ΔH^0 based on the slope and intercept.

The fitted coefficient of the Cr(VI) thermodynamic curve was greater than 0.95, indicating that the experimental and theoretical values were similar. The value of ΔG^0 decreases with increasing temperature, indicating a greater thermal driving force for the adsorption process of the composite. The positive value of the calculated ΔH^0 (21.0 kJ mol^{-1}) shows the heat-absorbing nature of the adsorption process. The adsorption reaction due to chemisorption is usually associated with ΔH^0

Table 3
Comparison of adsorption capacities of adsorbents for the removal of Cr(VI).

Adsorbent	Temperature °C	Adsorption Capacity mg g^{-1}	Wastewater treatment	Reference
UiO-66@/alginate beads	25	20.0	No	Daradmare et al. (2021)
Cr ion-imprinted polymer beads	25	250 ± 0.5	Yes	Elsayed et al. (2022)
PEI- INDION PA 800 beads	25	100.0	No	Verma et al. (2022)
Hollow PEI/carboxymethyl cellulose beads	25	535.39	No	Yang et al. (2021)
Nano iron oxides impregnated chitosan beads	25	92.04	No	Lu et al. (2021)
algal/alginate@PEI beads	25	380.0	No	Zhang et al. (2021)
Fe3O4/ZIF67@ aminated chitosan beads	25	119.05	No	Omer et al. (2021)
magnetic kaolin embedded chitosan beads	25	144.0	No	Liu et al. (2021)
triethylenetetramine-chitosan/alginate beads	25	291.3	No	Sharma et al. (2022)
EC-alg/PEI-3	25	769.2	Yes	This work

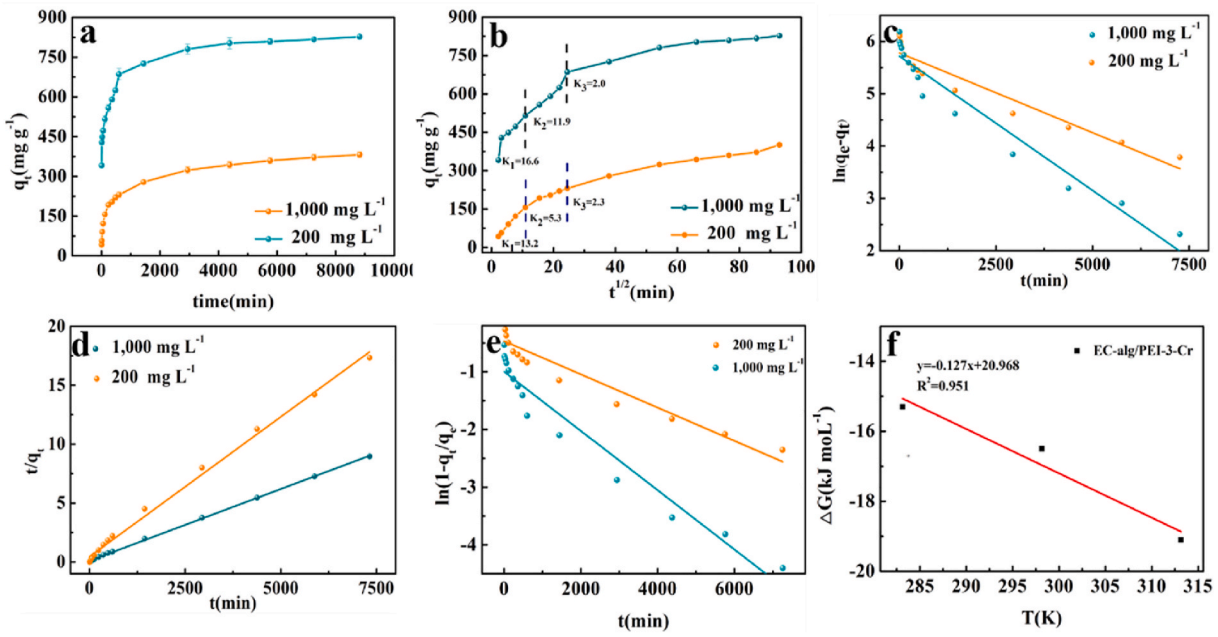

Fig. 5. Change in the adsorption capacity of EC-alg/PEI-3 with time**(a)**; Intraparticle diffusion model for Cr(VI) adsorption on EC-alg/PEI-3 **(b)**; Adsorption kinetics modeled with the pseudo-first-order equation **(c)** and Pseudo-second-order equation **(d)**; Boyd model of EC-alg/PEI-3**(e)**; Thermodynamic fitting curve of EC-alg/PEI-3**(f)**.

Table 4
Kinetic parameters of EC-alg/PEI-3 on Cr(VI).

	Intra-particle diffusion model						Boyd model	
Cr(VI) ppm	K_1 mg g^{-1} $min^{-1/2}$	R_1^2	K_2 mg g^{-1} $min^{-1/2}$	R_2^2	K_3 mg g^{-1} $min^{-1/2}$	R_3^2	D cm^2 s^{-1}	R^2
200	13.2	0.997	5.3	0.976	2.3	0.975	2.03×10^{-7}	0.967
1000	16.6	0.827	11.9	0.959	2.0	0.932	5.07×10^{-7}	0.947

Table 5
Thermodynamic parameters of EC-alg/PEI-3 on Cr(VI).

Temperature(°C)	ΔG^0 kJ mol^{-1}	ΔH^0 kJ mol^{-1}	ΔS^0 *k* J K^{-1} mol^{-1}
10	−15.3	21.0	0.13
25	−16.5		
40	−19.1		

in the range of 20–400 kJ mol^{-1}, as reported by Zhang et al. (2018). The value of ΔH^0 in this study indicates that the adsorption is mainly controlled by chemisorption. For an endothermic reaction, $\Delta H^0 < T\times\Delta S^0$ if the reaction can proceed spontaneously (Saad et al., 1995). During the adsorption of Cr(VI) on EC-alg/PEI-3, the quotient of $T\times\Delta S^0$ was more positive than ΔH^0, and the reaction could proceed spontaneously. During this reaction, the slightly positive ΔS^0 could originate from the energy redistribution between the adsorbate and the adsorbent. During the adsorption process, the structure of adsorbate and adsorbent molecules changes, and part of Cr(VI) is reduced to Cr(VI) or replaced with water molecules on the adsorbent surface to obtain additional transition entropy, which makes the system randomness increases (Gaurav et al., 2017). This part of the transition entropy increase may be slightly larger than the value of the entropy decrease caused by the adsorption of Cr(VI) by EC-alg/PEI-3, making the total entropy value of the system slightly positive.

3.9. Removal of Cr(VI) from electroplating wastewater by EC-alg/PEI-3

The actual electroplating wastewater chosen for this study had a pH

of approximately 2.4 and the concentration of Cr(VI) is about 216.2 ppm with complex composition. The main components were TN, COD, SO_4^{2-}, Cl^-, Ni^{2+}, Na^+ and Cu^{2+}, with concentrations of 61.3, 114, 646, 416, 47.6, 168, 19.6 ppm. To investigate the inhibitory effect of the presence of other components in the wastewater, a Cr(VI) solution was prepared with DI water at the same concentration as the Cr(VI) solution in the electroplating wastewater. At a solid-to-liquid ratio of 0.4 g L^{-1}, EC-alg/PEI-3 adsorbed 398.5 mg g^{-1} of Cr(VI) in the absence of competing ions. In the actual waste stream, EC-alg/PEI-3 adsorbed 307.6 mg g^{-1} of Cr (VI), which was approximately 77.2 % of the adsorption capacity in the absence of competing ions. The removal of Cr(VI) from the wastewater by EC-alg/PEI-3 was 94% when at dosage of 1 g L^{-1}, and when the dosage was increased to 1.4 g L^{-1}, the Cr(VI) concentration in the actual wastewater treated with EC-alg/PEI-3 was reduced to 0.041 ppm (Fig. 6b), which could meet the Chinese discharge requirements for industrial Cr(VI) wastewater.

3.10. Desorption experiments

The regenerative capacity of an adsorbent is an important parameter in practical applications. Adsorption of Cr(VI) by EC-alg/PEI-3 decreased with the number of cycles, with the adsorption amount starting at 318 mg g^{-1} in the first experiment, 260.3 mg g^{-1} in the second, and 148 mg g^{-1} in both the fifth and sixth experiments (Fig. 6a). This was probably due to the reduced number of amine groups and active sites in EC-alg/PEI-3. Notably, the bead structure was intact, indicating that beads had excellent mechanical properties and could be reused.

3.11. Adsorption mechanism of EC-alg/PEI-3 for Cr(VI)

In the SEM-EDS elemental mapping, Cr was uniformly distributed in the gel beads after adsorption of Cr(VI), visually proving that Cr was effectively adsorbed. First, under acidic conditions, the XPS map shows the appearance of protonated amino acid peaks on the surface of the EC-alg/PEI-3. After Cr(VI) adsorption, the protonated amine peak disappeared, indicating a clear electrostatic attraction between the Cr(VI) anion and the protonated amine. Second, after the adsorption of Cr(VI), new energy bands were observed (Fig. 3c), at 586 eV and 576 eV in the XPS pattern, which was formed by $Cr2p_{1/2}$ and $Cr2p_{3/2}$, indicating the presence of both Cr(VI) and Cr(III) in the adsorbed gel beads. At the same time, the XPS results indicated a shift in C–O and C=O, suggesting that carbon-oxygen groups are involved in the reduction of Cr(VI) to Cr (III) and that 530.2 eV is followed by a new peak Cr–O that may represent the possible binding of chromium to oxygen-containing groups (Kwak et al., 2020). The FTIR results showed that –CH, $–CH_2$, and –OH reduced Cr(VI) to Cr(III). To confirm that 25.7% of Cr(VI) was reduced to Cr(III) following EC-alg/PEI-3 adsorption, ICP-OES and UV spectrophotometry were used. This proves that redox reactions are essential for the adsorption of EC-alg/PEI-3. BET and SEM results showed that the EC-alg/PEI-3 gel beads had a rich 3D pore structure. In Fig. S2, the adsorption of the EC-alg/PEI powder was lower than that of the EC-alg/PEI-3 beads when the same material was used. This suggests that the multi-cavity structure of the alginate gel aids in the diffusion of Cr(VI) in the adsorbent material.

According to these analyses, the adsorption mechanism of Cr(VI) by EC-alg/PEI-3 can be speculated as follows. (1) Under acidic conditions, the amino groups on EC-alg/PEI-3 exist in the protonated form, and the negatively charged Cr(VI) anions are attracted to each other using positive and negative charges, leading to rapid adsorption of Cr(VI) by EC-alg/PEI-3 (Bao et al., 2020). (2) The surface amino group and internal hydroxyl group of EC-alg/PEI-3 acted as electron donor groups to reduce Cr(VI) to Cr(III) (Huang et al., 2022; Kwak et al., 2020), and the reduced Cr(III) was subsequently immobilized on the adsorbent surface by in situ chelation with N-containing groups.

$$-NH_3^+ + HCrO_4^- \rightarrow -NH_3^+ \ldots HCrO_4^- \quad (11)$$

$$Cr_2O_7^{2-} + 6e^- + 14H^+ \rightarrow 2Cr^{3+} + 7H_2O \quad (12)$$

$$HCrO_4^- + 3e^- + 7H^+ \rightarrow Cr^{3+} + 4H_2O \quad (13)$$

$$R - NH_2 + Cr^{3+} \rightarrow R - NH_2 \ldots Cr^{3+} \quad (14)$$

4. Conclusions

In this study, separable core-shell structured EC-alg/PEI-3 composite gel beads were prepared for the removal of Cr(VI) from water. At pH 2.0, the EC-alg/PEI-3 gel beads showed a maximum adsorption capacity of 714.3 mg g^{-1} at 10 °C and 769.2 mg g^{-1} at 25 °C. When treating actual electroplating wastewater with a complex composition, EC-alg/PEI-3 was less influenced by other components during adsorption and had an excellent anti-disturbance performance. In summary, EC-alg/PEI-3 is a promising adsorbent owing to its simple preparation process for mass production and ease of water separation, and it can be used for the treatment of specific industrial wastewaters.

CRediT authorship contribution statement

Yingnan He: Conceptualization, Methodology, Formal analysis, Validation, Writing – original draft. **Jianbing Chen:** Investigation, Data curation. **Jiapei Lv:** Investigation, Software. **Yimin Huang:** Investigation, Project administration. **Shuxing Zhou:** Resources, Investigation. **Wenyan Li:** Investigation. **Yongtao Li:** Validation. **Fengqin Chang:** Resources, Validation, Writing – review & editing. **Hucai Zhang:** Methodology. **Thomas Wågberg:** Validation, Formal analysis, Funding acquisition. **Guangzhi Hu:** Supervision, Funding acquisition, Writing – review & editing.

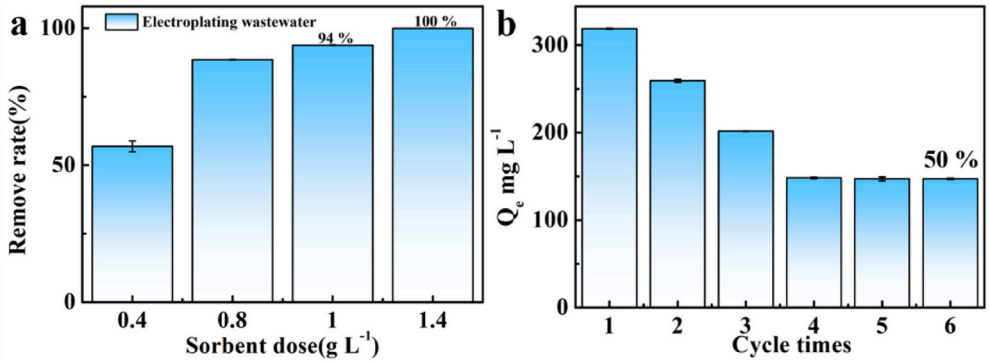

Fig. 6. The relationship between the dosage of EC-alg/PEI-3 and the removal rate of Cr(VI) in actual wastewater **(a)** and regeneration capacity of EC-alg/PEI-3 **(b)**.

Declaration of competing interest

The authors declare that they have no known competing financial interests or personal relationships that could have appeared to influence the work reported in this paper.

Data availability

The authors do not have permission to share data.

Acknowledgements

This work was financially supported by National Key R&D Program of China (2019YFC1804400), Special Project for Social Development of Yunnan Province (202103AC100001), Key Discipline of Materials Science and Engineering of Chizhou University (CZXYYLXK03), Anhui Province Materials and Chemical Industry First-class Undergraduate Talents Demonstration Leading Base (2020RCSFJDRCSFJD28), and Double First Class University Plan (C176220100042). T.W. acknowledges the support from Vetenskapsrådet (2017–04862, and 2021–04629). The authors thank the Advanced Analysis and Measurement Center of Yunnan University for the sample testing service.

Appendix A. Supplementary data

Supplementary data to this article can be found online at https://doi.org/10.1016/j.jclepro.2022.133790.

References

Asnam, A., Bouras, O., Aouabed, A., Bourven, I., Baudu, M., 2022. Structuration of biosorbents in the form of reinforced gelled and porous composites based on Opuntia ficus indica (cactus) extract and sodium alginate. Journal of Water Process Engineering 46.

Bajpai, J., Shrivastava, R., Bajpai, A.K., 2004. Dynamic and equilibrium studies on adsorption of Cr(VI) ions onto binary bio-polymeric beads of cross-linked alginate and gelatin. Colloids and Surfaces A: Physicochemical and Engineering Aspects 236 (1–3), 81–90.

Bao, S., Yang, W., Wang, Y., Yu, Y., Sun, Y., Li, K., 2020. PEI grafted amino-functionalized graphene oxide nanosheets for ultrafast and high selectivity removal of Cr(VI) from aqueous solutions by adsorption combined with reduction: behaviors and mechanisms. Chemical Engineering Journal 399.

Chen, P., Cheng, R., Meng, G., Ren, Z., Xu, J., Song, P., Wang, H., Zhang, L., 2021. Performance of the graphite felt flow-through electrode in hexavalent chromium reduction using a single-pass mode. Journal of Hazardous Materials 416, 125768.

Daradmare, S., Xia, M., Le, V.N., Kim, J., Park, B.J., 2021. Metal-organic frameworks/alginate composite beads as effective adsorbents for the removal of hexavalent chromium from aqueous solution. Chemosphere 270, 129487.

Elsayed, N.H., Monier, M., Alatawi, R.A.S., Albalawi, M.A., Alhawiti, A.S., 2022. Preparation of chromium (III) ion-imprinted polymer based on azo dye functionalized chitosan. Carbohydrate Polymers 284.

Fan, S., Zhou, J., Zhang, Y., Feng, Z., Hu, H., Huang, Z., Qin, Y., 2020. Preparation of sugarcane bagasse succinate/alginate porous gel beads via a self-assembly strategy: improving the structural stability and adsorption efficiency for heavy metal ions. Bioresource Technology 306, 123128.

Gaurav, S., Mu, N., Ala'a, H.A., Amit, K., Mohammad, R., Susheel, K., Shweta, M., Arush, S., 2017. Fabrication and characterization of chitosan-crosslinked-poly (alginic acid) nanohydrogel for adsorptive removal of Cr(VI) metal ion from aqueous medium. International Journal of Biological Macromolecules 95, 484–493.

González, B.Y., Rodríguez, R.I.L., Guibal, E., Calero de Hoces, M., Martín-Lara, M.Á., 2012. Biosorption of hexavalent chromium from aqueous solution by Sargassum muticum brown alga. Application of statistical design for process optimization. Chemical Engineering Journal 183, 68–76.

Guan, X., Zhang, B., Li, D., He, M., Han, Q., Chang, J., 2022. Remediation and resource utilization of chromium(III)-containing tannery effluent based on chitosan-sodium alginate hydrogel. Carbohydrate Polymers 284.

Han, S., Li, W., Xi, H., Yuan, R., Long, J., Xu, C., 2022. Plasma-assisted in-situ preparation of graphene-Ag nanofiltration membranes for efficient removal of heavy metal ions. Journal of Hazardous Materials 423 (Pt A), 127012.

Huang, Y., Lee, X., Grattieri, M., Macazo, F.C., Cai, R., Minteer, S.D., 2018. A sustainable adsorbent for phosphate removal: modifying multi-walled carbon nanotubes with chitosan. Journal of Materials Science 53 (17), 12641–12649.

Huang, Y., Wang, B., Lv, J., He, Y., Zhang, H., Li, W., Li, Y., Wågberg, T., Hu, G., 2022. Facile synthesis of sodium lignosulfonate/polyethyleneimine/sodium alginate beads with ultra-high adsorption capacity for Cr(VI) removal from water. Journal of Hazardous Materials 436.

Jia, W., Fan, R., Zhang, J., Geng, Z., Li, P., Sun, J., Gai, S., Zhu, K., Jiang, X., Yang, Y., 2022. Portable metal-organic framework alginate beads for high-sensitivity fluorescence detection and effective removal of residual pesticides in fruits and vegetables. Food Chemistry 377, 132054.

Kapur, M., Mondal, M.K., 2013. Mass transfer and related phenomena for Cr(VI) adsorption from aqueous solutions onto Mangifera indica sawdust. Chemical Engineering Journal 218, 138–146.

Karthik, R., Meenakshi, S., 2015. Removal of Cr(VI) ions by adsorption onto sodium alginate-polyaniline nanofibers. International Journal of Biological Macromolecules 72, 711–717.

Kong, L., Yan, R., Liu, M., Xu, J., Hagio, T., Ichino, R., Li, L., Cao, X., 2022. Simultaneous reduction and sequestration of hexavalent chromium by magnetic beta-Cyclodextrin stabilized Fe_3S_4. Journal of Hazardous Materials 431, 128592.

Kwak, H.W., Lee, H., Lee, K.H., 2020. Surface-modified spherical lignin particles with superior Cr(VI) removal efficiency. Chemosphere 239, 124733.

Lin, Z., Yang, Y., Liang, Z., Zeng, L., Zhang, A., 2021. Preparation of chitosan/calcium alginate/bentonite composite hydrogel and its heavy metal ions adsorption properties. Polymers (Basel) 13 (11).

Ling, L.L., Liu, W.J., Zhang, S., Jiang, H., 2017. Magnesium oxide embedded nitrogen self-doped biochar composites: fast and high-efficiency adsorption of heavy metals in an aqueous solution. Environmental Science & Technology 51 (17), 10081–10089.

Liu, D.M., Dong, C., Xu, B., 2021. Preparation of magnetic kaolin embedded chitosan beads for efficient removal of hexavalent chromium from aqueous solution. Journal of Environmental Chemical Engineering 9 (4).

Lu, J., Li, B., Li, W., Zhang, X., Zhang, W., Zhang, P., Su, R., Liu, D., 2021. Nano iron oxides impregnated chitosan beads towards aqueous Cr(VI) elimination: components optimization and performance evaluation. Colloids and Surfaces A: Physicochemical and Engineering Aspects 625.

Lv, X., Zhang, Y., Fu, W., Cao, J., Zhang, J., Ma, H., Jiang, G., 2017. Zero-valent iron nanoparticles embedded into reduced graphene oxide-alginate beads for efficient chromium (VI) removal. Journal of Colloid and Interface Science 506, 633–643.

Omer, A.M., Abd El-Monaem, E.M., Abd El-Latif, M.M., El-Subruiti, G.M., Eltaweil, A.S., 2021. Facile fabrication of novel magnetic ZIF-67 MOF@aminated chitosan composite beads for the adsorptive removal of Cr(VI) from aqueous solutions. Carbohydrate Polymers 265, 118084.

Omer, A.M., Khalifa, R.E., Hu, Z., Zhang, H., Liu, C., Ouyang, X.K., 2019. Fabrication of tetraethylenepentamine functionalized alginate beads for adsorptive removal of Cr (VI) from aqueous solutions. International Journal of Biological Macromolecules 125, 1221–1231.

Öztürk, A., Malkoc, E., 2014. Adsorptive potential of cationic Basic Yellow 2 (BY2) dye onto natural untreated clay (NUC) from aqueous phase: mass transfer analysis, kinetic and equilibrium profile. Applied Surface Science 299, 105–115.

Pi, S.Y., Wang, Y., Pu, C., Mao, X., Liu, G.L., Wu, H.-M., Liu, H., 2021. Cr(VI) reduction coupled with Cr(III) adsorption/precipitation for Cr(VI) removal at near neutral pHs by polyaniline nanowires-coated polypropylene filters. Journal of the Taiwan Institute of Chemical Engineers 123, 166–174.

Qiao, K., Tian, W., Bai, J., Zhao, J., Du, Z., Song, T., Chu, M., Wang, L., Xie, W., 2020. Synthesis of Floatable Magnetic Iron/biochar Beads for the Removal of Chromium from Aqueous Solutions, vol. 19. Environmental Technology & Innovation.

Qu, J., Wang, S., Jin, L., Liu, Y., Yin, R., Jiang, Z., Tao, Y., Huang, J., Zhang, Y., 2021. Magnetic porous biochar with high specific surface area derived from microwave-assisted hydrothermal and pyrolysis treatments of water hyacinth for Cr(VI) and tetracycline adsorption from water. Bioresource Technology 340, 125692.

Saad, A., Riaz-ur-Rehman, Ali, M., Khan, 1995. Adsorption of chromium (III), chromium (VI) and silver (I) on bentonite. Waste Management 15 (4), 271–282.

Sharma, P., Singh, S.P., Parakh, S.K., Tong, Y.W., 2022. Health hazards of hexavalent chromium (Cr (VI)) and its microbial reduction. Bioengineered 13 (3), 4923–4938.

Sivaraman, S., Michael Anbuselvan, N., Venkatachalam, P., Ramiah Shanmugam, S., Selvasembian, R., 2022. Waste tire particles as efficient materials towards hexavalent chromium removal: characterisation, adsorption behaviour, equilibrium, and kinetic modelling. Chemosphere 295, 133797.

Sun, X., Yang, L., Xing, H., Zhao, J., Li, X., Huang, Y., Liu, H., 2014. High capacity adsorption of Cr(VI) from aqueous solution using polyethylenimine-functionalized poly(glycidyl methacrylate) microspheres. Colloids and Surfaces A: Physicochemical and Engineering Aspects 457, 160–168.

Sun, X.F., Ma, Y., Liu, X.W., Wang, S.G., Gao, B.Y., Li, X.M., 2010. Sorption and detoxification of chromium(VI) by aerobic granules functionalized with polyethylenimine. Water Research 44 (8), 2517–2524.

Sun, Y., Liu, X., Lv, X., Wang, T., Xue, B., 2021. Synthesis of novel lignosulfonate-modified graphene hydrogel for ultrahigh adsorption capacity of Cr(VI) from wastewater. Journal of Cleaner Production 295.

Verma, R., Maji, P.K., Sarkar, S., 2022. Synthesis and validation of polystyrene-based polyethylenimine composite for Cr(VI) removal from aqueous solution: performance and mechanism. Journal of Environmental Chemical Engineering 10 (1).

Xiong, B., Wang, N., Chen, Y., Peng, H., 2018. Self-assembly of alginate/polyethyleneimine multilayer onto magnetic microspheres as an effective adsorbent for removal of anionic dyes. Journal of Applied Polymer Science 135 (7).

Yan, Y.Z., An, Q.D., Xiao, Z.-Y., Zhai, S.R., Zhai, B., Shi, Z., 2017. Interior multi-cavity/surface engineering of alginate hydrogels with polyethylenimine for highly efficient chromium removal in batch and continuous aqueous systems. Journal of Materials Chemistry A 5 (32), 17073–17087.

Yan, Y., An, Q., Xiao, Z., Zheng, W., Zhai, S., 2017. Flexible core-shell/bead-like alginate@PEI with exceptional adsorption capacity, recycling performance toward batch and column sorption of Cr(VI). Chemical Engineering Journal 313, 475–486.

Yang, H.R., Li, S.S., Shan, X.C., Yang, C., An, Q.D., Zhai, S.R., Xiao, Z.Y., 2021. Hollow polyethyleneimine/carboxymethyl cellulose beads with abundant and accessible

sorption sites for ultra-efficient chromium (VI) and phosphate removal. Separation and Purification Technology 278.
Yin, G., Tao, L., Chen, X., Bolan, N.S., Sarkar, B., Lin, Q., Wang, H., 2021. Quantitative analysis on the mechanism of Cd^{2+} removal by $MgCl_2$-modified biochar in aqueous solutions. Journal of Hazardous Materials 420, 126487.
Zhang, W., Wang, H., Hu, X., Feng, H., Xiong, W., Guo, W., Zhou, J., Mosa, A., Peng, Y., 2019. Multicavity triethylenetetramine-chitosan/alginate composite beads for enhanced Cr(VI) removal. Journal of Cleaner Production 231, 733–745.
Zhang, W., Zhang, S., Wang, J., Wang, M., He, Q., Song, J., Wang, H., Zhou, J., 2018. Hybrid functionalized chitosan-Al_2O_3@SiO_2 composite for enhanced Cr(VI) adsorption. Chemosphere 203, 188–198.
Zhang, Y., Mo, Y., Vincent, T., Faur, C., Guibal, E., 2021. Boosted Cr(VI) sorption coupled reduction from aqueous solution using quaternized algal/alginate@PEI beads. Chemosphere 281.
Zhao, N., Zhao, C., Liu, K., Zhang, W., Tsang, D.C.W., Yang, Z., Yang, X., Yan, B., Morel, J.L., Qiu, R., 2021. Experimental and DFT investigation on N-functionalized biochars for enhanced removal of Cr(VI). Environmental Pollution 291, 118244.
Zhao, N., Zhao, C., Lv, Y., Zhang, W., Du, Y., Hao, Z., Zhang, J., 2017. Adsorption and coadsorption mechanisms of Cr(VI) and organic contaminants on H_3PO_4 treated biochar. Chemosphere 186, 422–429.
Zhao, X., Zheng, J., You, S., Du, L., Liu, C., Chen, K., Liu, Y., Ma, L., 2021. Selective adsorption of CR (VI) onto amine-modified passion fruit. Peel Biosorbent. Processes 9 (5).
Zheng, Z., Duan, X., Tie, J., 2022. One-pot synthesis of a magnetic Zn/iron-based sludge/biochar composite for aqueous Cr(VI) adsorption. Environmental Technology & Innovation 28, 102661.
Zhuang, Y., Yu, F., Chen, H., Zheng, J., Ma, J., Chen, J., 2016. Alginate/graphene double-network nanocomposite hydrogel beads with low-swelling, enhanced mechanical properties, and enhanced adsorption capacity. Journal of Materials Chemistry A 4 (28), 10885–10892.